IEEE Access
Multidisciplinary | Rapid Review | Open Access Journal

Received October 11, 2018, accepted October 25, 2018, date of publication October 31, 2018, date of current version December 3, 2018.

Digital Object Identifier 10.1109/ACCESS.2018.2878904

A Coaxial Dipole Antenna for Passively Sensing Object Displacement and Deflection for Orthopaedic Applications

KEVIN M. LABUS[1], BRANISLAV M. NOTAROŠ[2], (Fellow, IEEE), MILAN M. ILIĆ[3], (Senior Member, IEEE), CONOR J. SUTHERLAND[1], AMY HOLCOMB[1], AND CHRISTIAN M. PUTTLITZ[1]

[1]Department of Mechanical Engineering, Colorado State University, Fort Collins, CO 80523, USA
[2]Department of Electrical and Computer Engineering, Colorado State University, Fort Collins, CO 80523, USA
[3]School of Electrical Engineering, University of Belgrade, 11120 Belgrade, Serbia

Corresponding author: Branislav M. Notaroš (notaros@colostate.edu)

This work was supported in part by the National Science Foundation under Grant ECCS-1307863.

ABSTRACT A promising approach for monitoring and predicting the course of bone fracture healing is by measuring the mechanical load-sharing between the healing callus and the implanted fixation hardware. Previous technologies have used implantable sensors which require modification to the fixation hardware and may carry long term biocompatibility risks. The objective of this paper was to optimize and evaluate a method of externally sensing hardware load-sharing based on the electromagnetic near field effects of a radio-frequency antenna. A series of parametric experiments was conducted to optimize the dimensional parameters of a coaxial dipole antenna to improve the antenna's sensitivity to displacement of a metal plate. The results of the parametric tests guided the design of an optimized antenna, including a coiled loop antenna structure. The antenna was then evaluated for its efficacy in sensing the displacement of a metal plate as well as the deflection of an orthopaedic fracture fixation plate due to an applied load via physical experiments and computational simulations. The antenna's resonant frequency was sensitive to the displacement of a metal plate, and followed an inverse-square relationship with plate distance. The antenna was also able to sense the bending deflection of the mechanically loaded fracture plate, with the resonant frequency following an approximately linear relationship with applied load. Computational finite-element electromagnetic predictions closely matched the experimental data. This method of sensing plate deflections may be effective for measuring the mechanical load sharing in fractured bones in order to monitor and predict the course of fracture healing.

INDEX TERMS Antenna for orthopaedic application, antenna resonant frequency, computational electromagnetic simulations, coaxial dipole antenna, electromagnetic sensor, external sensing of object displacement and deflection, finite element method, monitoring and predicting bone fracture healing, near electromagnetic field, RF measurements.

I. INTRODUCTION

Orthopaedic extremity injuries are commonly associated with complications, with about 10% of fractures in the United States failing to heal properly [1]. The most common complication, bony non-union, is a chronic condition associated with pain and disability. The deleterious effects and resultant costs of non-unions can be reduced by an estimated 50% if the non-union can be avoided or addressed during the early time period of healing [2]. Therefore, it is critical to monitor the course of healing and to have the capability to diagnose non-unions in the early time period. Currently, the progress of fracture healing is typically monitored using radiographs. However, abnormal healing is not easily diagnosed radiographically during the early time period due to the relative paucity of mineralized tissue [3]. Therefore, new technologies that are capable of diagnosing abnormal healing early in the process could potentially improve the treatment of fractures at risk of non-union.

The normal healing process of a fracture is characterized by an increasing stabilization of the fracture during the early time period [4]–[6]. This stabilization coincides with temporal shifts in the mechanical load-sharing profile between the implanted fixation hardware (typically plates with screws or intramedullary nails) and the native bone and callus. Animal studies using strain gauges to measure implant loading have demonstrated that the relative load carried by the implant decreases over time as the fracture heals and the callus and bone carry an increasing share of the load [7]. For non-unions or other abnormal healing, this temporal trend in load sharing is delayed or non-existent because the healing bone does not have the structural ability to assume a healthy share of the load. Therefore, measuring temporal changes in implant loading is a promising approach to distinguish between normal and aberrant healing for diagnostic purposes.

A number of implantable sensors have been developed for monitoring fracture healing. One approach utilized a strain sensor integrated into a fixation plate, allowing for precise strain measurements in an *in vivo* rodent model [8], but the wireless data transmission requires a bulky implanted transceiver, limiting the potential for clinical translation. Our group has developed a radio-frequency (RF) electromagnetic coupling system that utilizes a biocompatible, microelectromechanical system (bioMEMS) sensor [9]–[17]. The sensor is essentially a wireless strain gauge that is attached to the internal hardware device (either plate or intramedullary nail) used to fix the fracture. The sensor is electromagnetically coupled to an external antenna producing a particular resonance (in the MHz range), and this resonance shifts as the plate (and, therefore, the attached sensor) is loaded and deformed. Accordingly, we have developed this system to telemetrically measure the *in vivo* loading profile at the fracture site, and we have shown that these data can be used to predict the course of fracture healing in a large animal model [18]. However, implanted sensors carry potential biocompatibility issues and require modification to the implanted hardware, which can limit their clinical adoption [19].

In the scenario of a fractured long bone fixed with a plate and screws, a compressive axial load on the construct can cause the plate to bend. When probing the bioMEMS sensor, the lateral deflection of the plate due to bending may alter the resonance of the external antenna. Therefore, we hypothesize that the external antenna can directly couple with the fixation hardware with no implanted sensor (''direct electromagnetic coupling'', DEC) and sense the relative load on the hardware via deflections causing a shift in resonant frequency. The advantages of this ''sensorless'' technique over the bioMEMs sensor method is that it (1) eliminates the implementation of a sensor with the hardware (i.e. attachment); (2) eliminates long-term biocompatibility issues associated with the sensor materials and potential *in vivo* breakdown; and (3) can be used with any hardware configuration.

The electromagnetic properties of radio-frequency antennas are dependent on the environment, and can be altered by objects located in the near field. Metal objects in the near field of an antenna alter the many antenna properties and change the resonant frequency of the antenna [20]. Non-metallic, non-conductive objects can also alter the performance of radio-frequency antennas through dielectric effects [21]–[23]. In many applications, such as RFID, the electromagnetic near field effects are often studied in the context of performance reductions [22], [24]. Alternatively, antennas can be designed to leverage this phenomenon and maximize the sensitivity for a specific application. These near field effects have been investigated to use antennas as proximity sensors, to detect the presence of an object [20], [25], and non-contact displacement sensors for industrial applications [26], [27]. There may be further potential to optimize an antenna to sense mechanical deformations and deflections of a structural object, particularly for orthopaedic applications, requiring high precision sensing of implant deflections of less than 1 mm.

The objectives of this study were to investigate the dimensional parameters of a radio-frequency antenna and the effects on sensitivity to a metal plate in the near field, and to test an optimized antenna design for use as a sensor to monitor fracture healing. The antenna was tested via physical experiments and computational modeling for its efficacy to sense displacements of a metal plate and to sense deflections in an orthopaedic fracture fixation plate under an applied mechanical load.

II. STUDY OVERVIEW

Previous work by our group used a custom antenna to probe a passive strain sensor [18]. The antenna consisted of two parallel coaxial cables, approximately 1 m in length, with the outer conductor removed over a length of 4 cm at the end of each cable. The outer shielding of the two cables was electrically connected at their other terminus to facilitate noise minimization from the lead cable, which connected the antenna to the network analyzer. Because this antenna type was observed to be highly sensitive to objects in the near field, it was chosen for optimization as an object displacement sensor for the intended application and current study.

This study included a series of two parametric tests intended to optimize the sensitivity of the antenna to the displacement of a metal plate. The parameters tested were the placement of the plate along the length of the antenna and the spacing between the two coaxial cables. These parametric tests are presented first, along with their results, which formed the basis for a new antenna design. The resulting antenna underwent two tests to determine its efficacy for sensing the displacement of a metal plate and the deflection of a metal orthopaedic plate in a modeled fracture condition. The physical experiments were augmented with mechanical finite element and electromagnetic computational simulations.

For all tests in this study, a vector network analyzer (model: TTR503A, Tektronix, Beaverton OR) was used to create an excitation in the antenna with a power of 7 dBm (5 mW) and to measure the response of the $|S_{11}|$ parameter (return loss).

The target object (metal plate) in the vicinity couples with the antenna and alters the electromagnetic near field, thus shifting the apparent resonant frequency (ARF) as determined from the measured $|S_{11}|$ parameter. The ARF was defined as the frequency at which the $|S_{11}|$ sweep reaches a minimum in the response magnitude (dB) within the frequency measurement range.

III. ANTENNA PARAMETRIC TESTS

A. PARAMETRIC TEST ON PLATE LOCATION ALONG LENGTH OF ANTENNA

A parametric test was conducted to determine the location(s) along the length of the antenna that were most sensitive to the placement of a metal plate (*i.e.,* resulted in the greatest shift in ARF). Each of the antenna's coaxial cables were 120 cm long and spaced 15 mm apart. At one end of the cables, the outer conductors (shielding) were removed over a 5 cm length (Fig. 1). On the other terminus, the two outer conductors were electrically connected to each other, and one of the cables was connected to the network analyzer via a lead cable. The antenna was fixed in a straight line to a polycarbonate board, and the board was placed on a wood tabletop.

A baseline frequency sweep was recorded in free space with no objects in the vicinity of the antenna. The frequency sweeps spanned each of the first three observed harmonic resonant frequencies, occurring at approximately 85 MHz, 179 MHz, and 275 MHz. A stainless steel plate (with dimensions 12.7 mm × 6.34 mm × 152 mm) was placed on top of the antenna, across the two cables, and displaced by 1 cm increments along the entire length of the antenna (Fig. 1). At each increment, frequency sweeps were recorded at each harmonic, and the ARF was determined.

At most locations on the antenna, the placement on the plate produced a decrease in the measured ARF. The first, second, and third harmonic resonant frequencies exhibited one, two, and three local minima in the ARF, respectively, along the length of the antenna, representing the locations of the greatest magnitude frequency shifts (Fig. 1). These locations of greatest sensitivity, and the associated ARFs, are shown in Table 1. The third harmonic exhibited the greatest ARF shifts when normalized to the baseline (free space) ARF. At all three harmonics, there was one location of high sensitivity at 7 or 8 cm from the end of the antenna, just beyond the 5 cm section where the outer shielding was removed.

B. PARAMETRIC TEST ON CABLE SPACING

A stainless steel plate (with dimensions 12.7 mm × 6.34 mm × 152 mm) fixed to a polymeric bar was connected to a linear actuator (T-LLS105, Zaber Technologies, Vancouver, BC, Canada), and a 100 cm long antenna was fixed to the stationary frame of the actuator such that one of the locations of greatest sensitivity (as determined by the plate placement parametric test) was aligned with the stainless steel plate (Fig. 2a). Pilot experiments using antennas with different total lengths demonstrated that the locations of

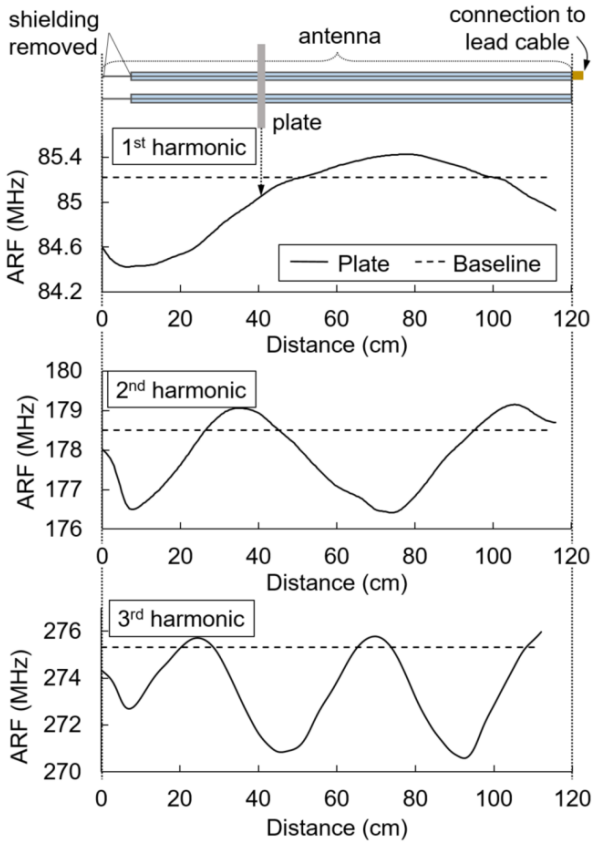

FIGURE 1. The ARF is plotted for the first three harmonic resonant frequencies as the distance of the stainless steel plate from the end of the antenna changes. The x-axes are representative of the plate placement on the antenna as shown in the diagram (top). The baseline represents the measurement in free space (with no plate). The local minima of each plot correspond to the locations of greatest sensitivity of the antenna.

TABLE 1. Distance along the antenna length and resonant frequencies of the locations where the plate placement cause the greatest shift in ARF. Locations are defined as the distance from the end of the antenna where the outer shielding is removed.

	Location of greatest shift (cm)	*Location (percent of total length)*	*ARF (MHz)*	*ARF shift from baseline (MHz)*	*ARF shift (percent of baseline)*
1st Harmonic	7	6%	84.423	-0.796	-0.93%
2nd Harmonic	8	7%	176.498	-2.010	-1.13%
	74	62%	176.417	-2.091	-1.17%
3rd Harmonic	7	6%	272.691	-2.633	-0.96%
	46	38%	270.836	-4.488	-1.63%
	93	78%	270.579	-4.745	-1.72%

greatest sensitivity were linearly proportional to the antenna length. Accordingly, for tests of the first, second, and third harmonic frequencies, the plate was aligned 6 cm, 62 cm, and 38 cm from the end of the antenna, respectively, for this 100 cm long antenna. The antenna cables were threaded

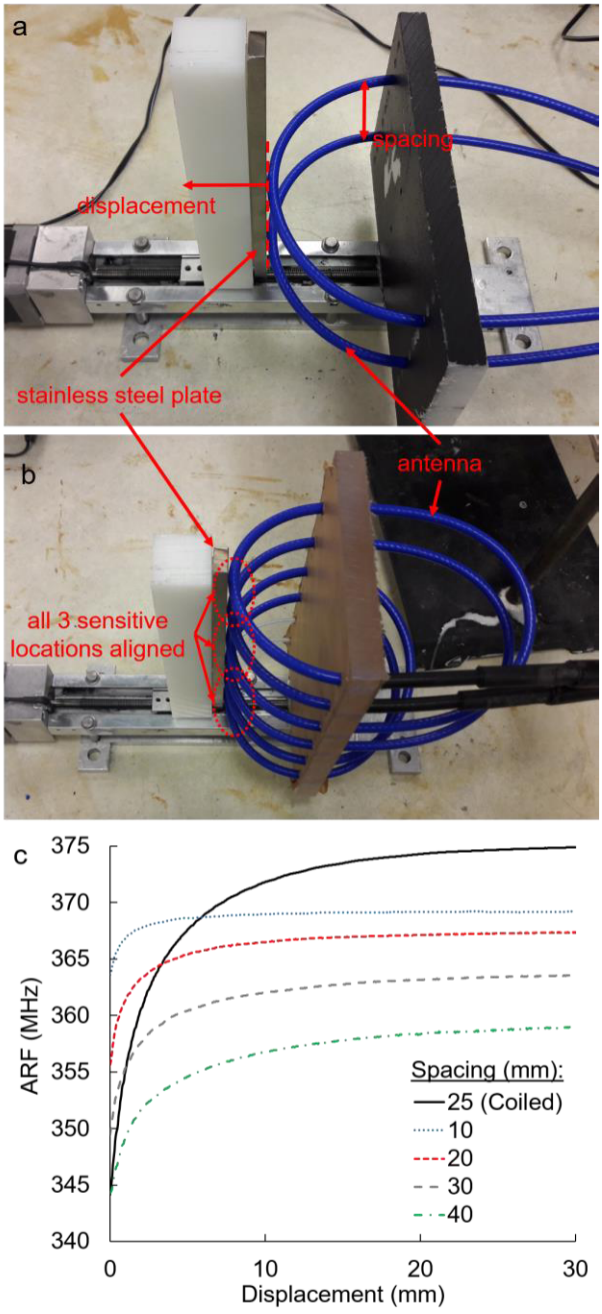

FIGURE 2. (a) For the parametric test of cable spacing, the blue antenna cables here held fixed to the linear actuator frame as the stainless steel plate was displaced away from the antenna. (b) The coiled antenna used three loops of each cable to align all three (third harmonic) sensitive locations of the antenna in front of the plate. (b) Example ARF versus displacement curves for all third harmonic tests and the coiled antenna test. At 10 mm spacing the ARF increased sharply at low displacements, then quickly plateaued. As the cable spacing increased, the overall ARF shifts were greater, and the ARF increased at a more even rate as displacement increased. The coiled antenna showed far greater shifts in ARF compared to the other tests.

through holes in a polymeric plate to test the cable spacing fixed at 10 mm, 20 mm, 30 mm, and 40mm between the central axes. To conduct each test, the plate was initially in contact with both antenna cables and then displaced up to 30 mm away from the antenna. ARF was continuously recorded from frequency sweeps every 0.04 mm. A final test was conducted with the same antenna cables coiled into three loops, with a 25 mm spacing, such that all three of the third harmonic locations of greatest sensitivity (6 mm, 38 mm, and 78 mm) were radially aligned on the side of the antenna adjacent to the plate (Fig. 2b). To describe the relationship between ARF and displacement (u), the data were fitted with a simple inverse-square model:

$$\text{ARF} = \frac{c}{(u+u_0)^2} + f_\infty \tag{1}$$

where c is a sensitivity coefficient, u_0 is an initial displacement offset, and f_∞ is the resonant frequency as $u \to \infty$.

At all harmonics and cable spacings tested, the ARF increased as the plate was displaced away from the antenna (Fig. 2c). The relationship between ARF and displacement was highly nonlinear, with the ARF sensitivity deceasing at greater plate displacements, and the curves were very well fitted by the inverse square model (mean RMSE = 0.12 MHz, which represented 1% of the mean ARF shift from 0 to 30 mm). The c parameter of the inverse square model, which is representative of sensitivity, increased in magnitude as the cable spacing increased (Fig. 3a). The c parameter also increased as the harmonic increased from one to three, which may be partly due to the higher harmonics being located at higher frequencies. The coiled antenna exhibited the greatest c parameter. The u_0 parameter also increased as cable spacing increased, but did not show a consistent trend with respect to harmonic level (Fig. 3b). A greater u_0 parameter generally affected the inverse square model by decreasing the sensitivity (ARF/displacement slope), but also resulted in a lesser degree of decreasing sensitivity as the plate was moved away from the antenna. In other words, the trend of increased c and increased u_0 as cable spacing increased was representative of the shape of the curves having a greater degree of linearity and greater overall ARF shifts (Fig. 2c), which are desired characteristics for using the antenna as a displacement sensor.

The overall ARF shifts from 0 to 30 mm (as a percent of frequency magnitude) showed an increasing trend as the cable spacing increased (Fig. 3c), and was greatest for the coiled antenna (about two times greater than the mean of the other tests). The signal-to-noise ratio did not follow a consistent trend with respect to spacing or harmonic level, but it was about five times greater for the coiled antenna than for the next greatest test (Fig. 3d). The signal-to-noise ratio was defined as the ARF shift from 0 to 30 mm, divided by the maximum amplitude of random noise from 29.5 mm to 30 mm, where the ARF was relatively unaffected by displacement.

IV. METHODS

A. COILED ANTENNA DESIGN

Based on the results of the parametric tests, an antenna was designed to measure deflections of an orthopaedic fracture fixation plate. Due to its relatively high sensitivity, the coiled third harmonic antenna concept was used. The cable spacing and length were restricted due to size constraints of the bones

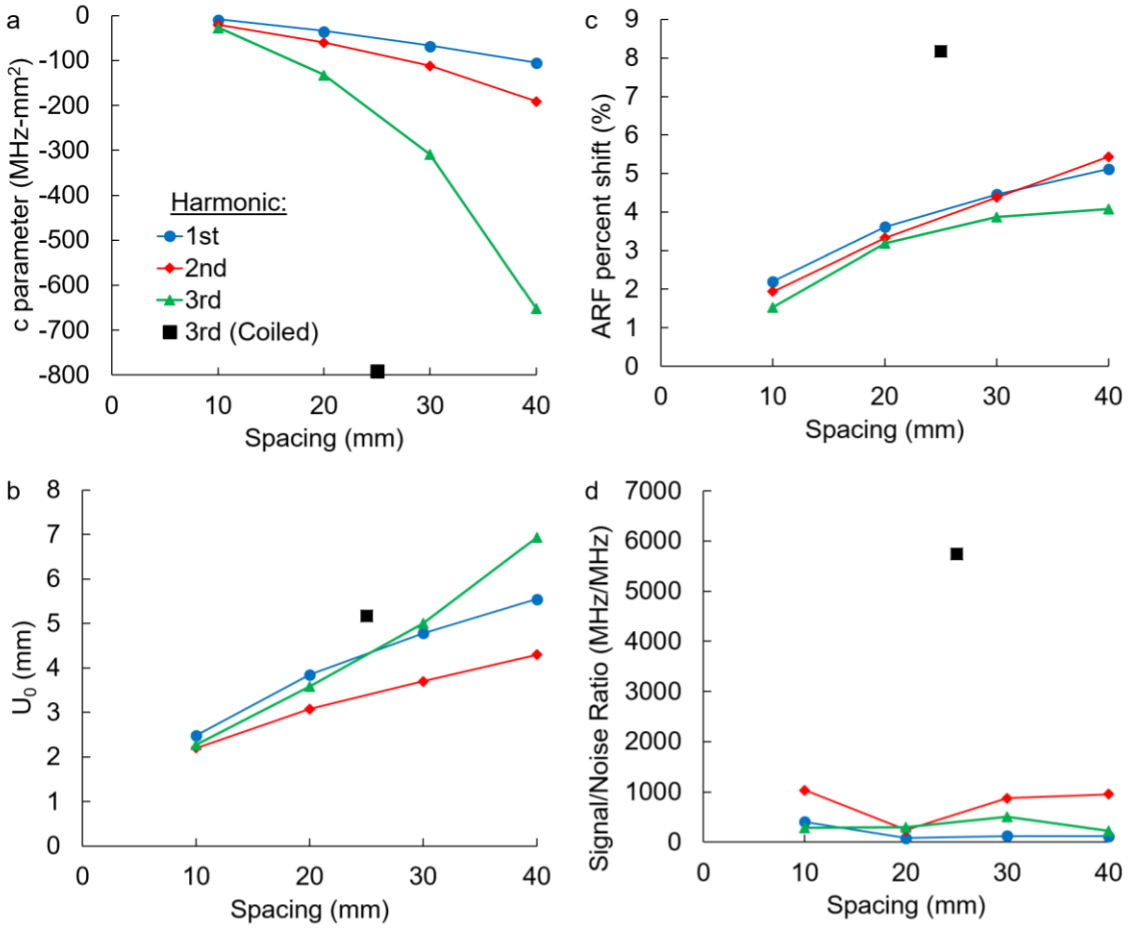

FIGURE 3. The ARF versus displacement curves from the parametric tests on cable spacing were analyzed to show the effects of the spacing. (a) The *c* parameter (sensitivity) of the inverse square model increased with greater spacing and greater harmonic levels, and was greatest for the coiled antenna. (b) The *u0* parameter (initial displacement) of the inverse square model increased with greater spacing. (c) The overall ARF shift, between 0 and 30 mm, as a percent of the ARF at 30 mm showed an increasing trend as the spacing increased, and was greatest for the coiled antenna. (d) The signal/noise ratio was greatest for the coiled antenna. Together, these data indicate that greater spacing resulted in greater sensitivity of the ARF to changes in plate displacement. Also, by aligning three sensitive locations of the antenna resulted in greater overall sensitivity.

and plates to be measured. The antenna used two 85 cm long coaxial cables, each coiled into three loops such that all three third harmonic locations of greatest sensitivity were aligned, and the cables were spaced 15 mm apart (Fig. 4). The antenna cables were held in place by a polycarbonate frame. The frame also included two contact points spaced 7 mm from the edge of the antenna cables to hold the antenna at a fixed location relative to the target object (a fractured bone fixed with a plate). This antenna was used for all subsequent tests.

B. COILED ANTENNA: PLATE DISPLACEMENT TEST

Similar to the cable spacing parametric test, the effect of a plate displacement on the antenna's ARF was measured. A stainless steel plate (with dimensions 12.7 mm × 6.34 mm × 152 mm) was attached to a linear actuator (T-LLS105, Zaber Technologies, Vancouver, BC, Canada). The antenna was kinematically constrained and held at a constant location. The antenna's frame was in contact with the surface of the plate, which placed the edge of the antenna cables 7 mm from the surface of the plate at the initial position (zero displacement). The plate was then linearly displaced away from the antenna up to 50 mm while recording the displacement of the plate and performing frequency sweeps (411 MHZ – 441 MHz) of the $|S_{11}|$ parameter from the antenna. A second stainless steel plate (12.7 mm × 6.34 mm × 87.7 mm) was attached to the existing metal plate and the test was repeated (double plate). The shorter length of the second plate allowed for the stainless steel surface to fit between the antenna's contact points and maintain an initial position which was closer to the cables (0.66 mm) to determine the sensitivity in very close proximity. The test was repeated a third time with no plate attached to the linear actuator in order to determine what electromagnetic resonance effects, if any, the actuator itself had on the antenna. The ARF versus displacement data were fitted with a simple inverse-square model (equation 1).

For the electromagnetic modeling and analysis, the DEC system was represented as general three-dimensional

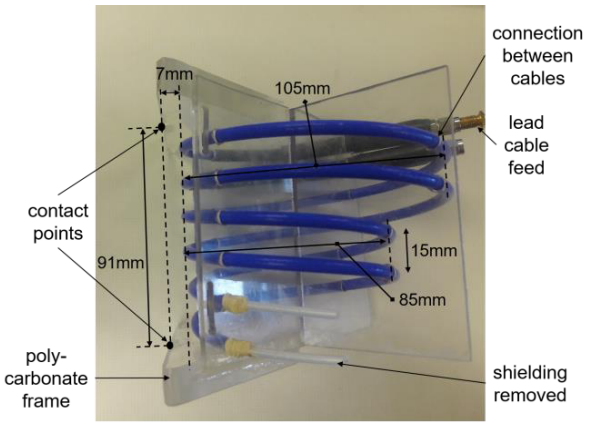

FIGURE 4. The coiled loop antenna was designed for sensing deflections of a fracture fixation plate under a mechanical load. The three third harmonic locations of greatest sensitivity were radially aligned (left side of photograph). The cables were held in place with a frame that included contact points for placing the antenna against the target object (fractured bone).

electromagnetic structure composed of metallic wires, metallic surfaces, and dielectric bodies. The chosen modeling approach was to solve partial differential equations (PDEs), namely Maxwell's equations or their combinations (wave equations) [28], directly for the relevant electromagnetic fields throughout the volume of the structure and the remaining computational domain via the finite element method (FEM) [29]. FEM provides unparalleled versatility in modeling of material inhomogeneity and complexity, which is convenient for detailed electromagnetic modeling of biological tissues. We adopted a commercial FEM software suite (High Frequency Structure Simulator (HFSS), v. 17.0.0, ANSYS Inc, Canonsburg, PA) as the final solver for this study to make the results more repeatable and the model properties more understandable, using a commercially available code, namely, arguably the most widely used computational electromagnetic tool for antenna analysis and design and other kinds of electromagnetic modeling.

The single stainless steel plate experiment was simulated by constructing a simple model of the antenna and the rectangular plate (Fig. 5a). The models were built from tetrahedral finite elements in conjunction with field expansions of first orders. The FEM mesh was terminated using a second-order absorbing boundary condition [30], and the simulations were run with adaptive mesh refinement and an iterative solver employing recursive updates until tolerance was reached. An air box enclosed the complete antenna setup and provided the computational domain boundaries. The second-order absorbing boundary condition was applied to the air box faces, thus simulating the infinite open space around the modeling domain.

C. ORTHOPAEDIC PLATE COMPRESSION TEST

When a fractured long bone fixed with a plate and screws is loaded in axial compression, the offset of the plate from the line of loading causes the plate to experience a bending moment and a lateral deflection (Fig. 6a). To test the efficacy of the DEC system to sense the deflection of the plate, a physical experiment was conducted to replicate the mechanical environment of a fractured long bone, and corresponding mechanical and electromagnetic computational simulations

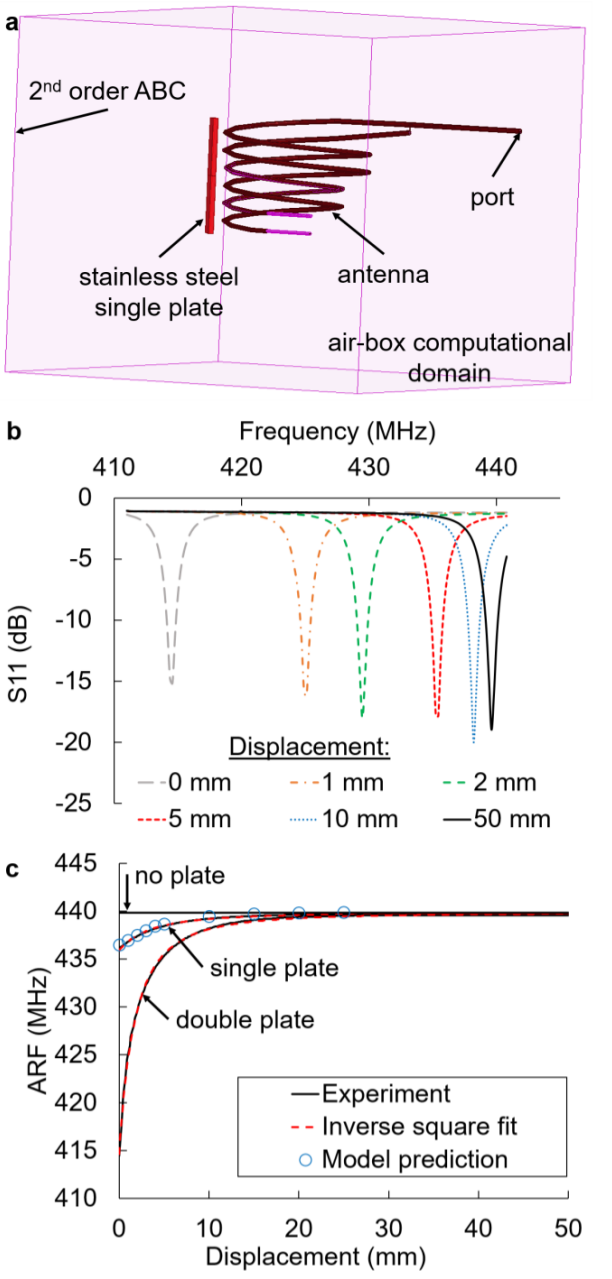

FIGURE 5. (a) Electromagnetic model setup of the plate displacement test with the antenna and stainless steel single plate enclosed in an air box modeling domain. (b) Example frequency sweeps of $|S_{11}|$ for the double plate test show clear frequency shifts as the displacement changes. (c) Relationship between ARF and stainless steel plate displacement, showing experimental data, fits of an inverse square model, and electromagnetic model predictions. The electromagnetic model and inverse square fitting procedure closely approximated the experimental results.

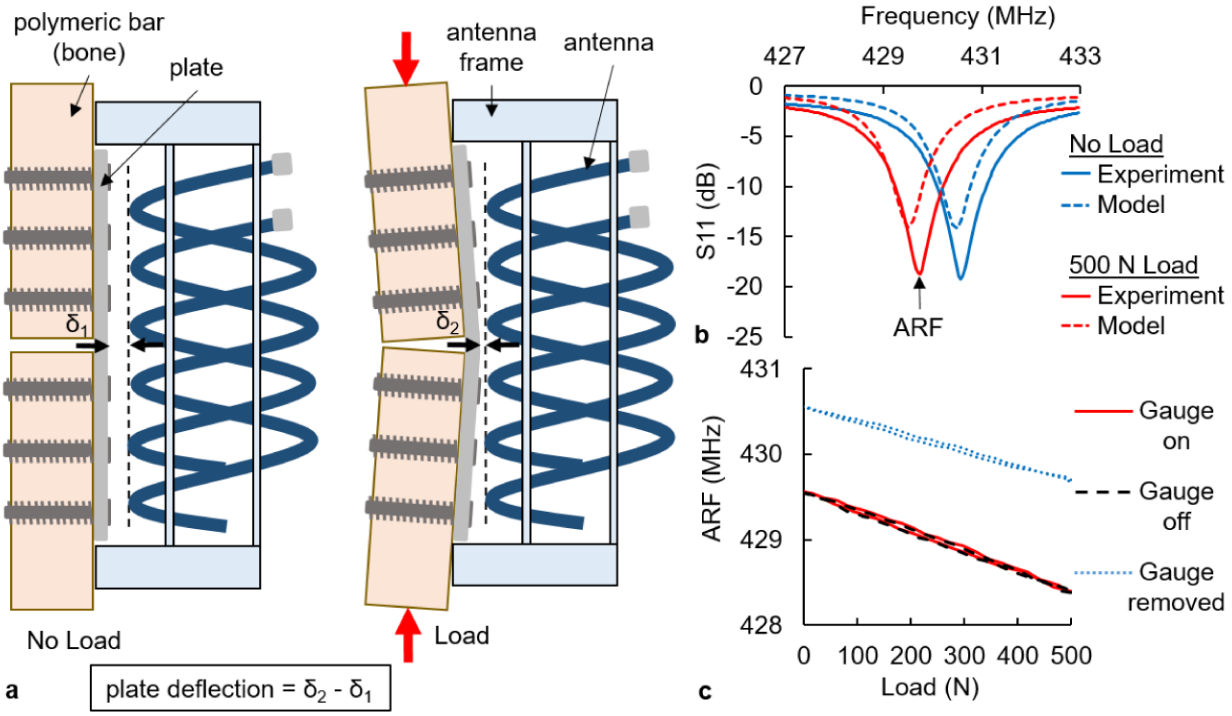

FIGURE 6. (a) Diagram demonstrating bending of a fracture fixation plate due to a compressive load and the resulting deflection of the plate relative to the antenna. This displacement produces a shift in the measured ARF. (b) $|S_{11}|$ frequency sweeps of the construct in (A) under 0 N and 500 N of load for the plate compression test and corresponding electromagnetic modeling results. ARF was obtained at the minima of the frequency sweep (as indicated by the black arrow for the 500 N experimental curve. (c) ARF versus load curves from the plate compression test comparing the effects of the strain gauge.

were performed. A compressive test of an orthopaedic fracture fixation plate attached to a polymeric bar was conducted due to its relative ease in modeling and to test the DEC coupling technique as applied to a configuration that is similar to potential future bone fracture applications.

An acetal polymer bar (Delrin®, 25 mm × 25 mm × 250 mm) was cut into two pieces to model two segments of bone and a transverse mid-diaphyseal fracture. The acetal material exhibits a relative permittivity (3.6) that is similar to that of bone [31]. A six-hole fracture fixation locking plate (P04028, Synthes, West Chester, PA) was fastened to the bar such that there was a simulated 8 mm ''fracture'' gap. A strain gauge rosette (MMF313001, Micro Measurements, Raleigh, NC) was attached to the center of the plate on the outer surface. The antenna was secured to the construct such that the antenna casing was in contact with fixed points on the acetal bar on either end of the plate. The construct was loaded in 500 N of compression for five cycles while measuring the plate's principal strain, applied load, and ARF. The test was repeated with the strain gauge unplugged from its source to determine the effect, if any, of the strain gauge current on the electromagnetic near field. The test was repeated a third time with the strain gauge removed to determine the effects of the strain gauge's physical presence and how these data compared to the electromagnetic modeling predictions.

A corresponding computational simulation was performed in order to predict the degree of plate deflection associated with the measured strain measurements. A finite element model was constructed which replicated the geometry of the acetal bar-plate construct. The solid model was developed using SolidWorks (2016 x64 Edition, Dassault Systemes, Waltham, MA), and ABAQUS (2017, Dassault Systemes, Waltham, MA) was utilized to prescribe the loading conditions and perform the analysis. The bottom aspect of one of the acetal components had an encastre boundary condition imposed while the top surface was subjected to a 500 N axial load. Principal strain was predicted from a group of 34 surface nodes on the outer face of the plate, which corresponded to the location of the strain gauge in the experimental testing. The relative deflection of the plate was predicted and defined as the lateral displacement of a node on the center of the plate relative to the line connecting two nodes at the contact points of the antenna housing, located 45 mm above and below the center of the plate. The angle of deflection of the bending plate was also predicted for the purpose generating the deformed electromagnetic model.

An electromagnetic computational model was constructed to simulate the plate compression test. The simulations used the same antenna model geometry as was utilized in the proximity test, and the acetal bar-plate construct was included in both its unloaded and loaded configurations. The model enables simple adjustment of the bar bend angle through parametric modeling. To replicate the bending of the plate under loading, the deformed (under 500 N load) geometry

predicted by the mechanical finite element simulation was used to define a bend angle of 1.46 degrees. The $|S_{11}|$ parameter responses were predicted for frequency sweeps of each model.

V. RESULTS

A. COILED ANTENNA: PLATE DISPLACEMENT TEST

The measured frequency sweeps of $|S_{11}|$ showed a distinct increase in the resonant frequency as the plate was displaced away from the antenna (Fig. 5b). The double plate, which had a closer initial position to the antenna, exhibited a greater shift in ARF than the single plate (Fig. 5c). Additionally, the nonlinear ARF versus displacement curves exhibited a greater sensitivity as the distance from the antenna decreased. The data were fitted well by the inverse square model (RMSEs of the single plate and double plate tests were 0.04 MHz and 0.14 MHz, respectively). The fitted parameters were $c = -197$ MHz-mm^2, $u_0 = 7.1$ mm, and $f_\infty = 439.9$ MHz for the single plate test, and $c = -316$ MHz-mm^2, $u_0 = 3.5$ mm, and $f_\infty = 439.9$ MHz for the double plate test. The greater absolute magnitude for c and lower u_0 of the double plate confirmed the greater sensitivity for that configuration. The test with no plate showed no detectable shift in ARF, which matched the fitted f_∞ values of the single plate and double plate tests, indicating that the actuator itself had a negligible effect on the antenna. In free space (50 mm displacement), the Q-factor of the antenna was measured to be 400, defined as the ARF divided by the bandwidth at half the peak amplitude. The electromagnetic computational simulations very closely predicted the ARF obtained by experimental measurements (RMSE = 0.22 MHz). The slight ''oscillation'' of simulated results about the experimental curve can be attributed to differences in the actual FEM meshes for electromagnetic computation used to obtain each of the results, which, in turn, yield slightly different solution accuracies (residuals of full wave FEM numerical solutions).

B. ORTHOPAEDIC PLATE COMPRESSION TEST

The compressive load applied to the acetal bar and orthopaedic plate construct produced a tensile strain (cyclic mean $\pm$ standard deviation: 1353 $\mu\varepsilon\pm$ 6 $\mu\varepsilon$) on the outer surface of the plate under a 500 N load, which indicates that the plate was experiencing substantial bending due to the relative position of the applied compressive load with respect to the neutral axis of the acetal bar/plate construct. The deflection of the plate towards the antenna resulted in a decrease in the plate's ARF. The ARF versus applied load curve was highly linear (linear regression $r^2 > 0.995$) and was calculated for each of the experimental tests (Fig. 6c). For the tests with the strain gauge on, strain gauge turned off, and strain gauge removed, the resultant slopes of the ARF versus applied load curves were (cyclic mean $\pm$ standard deviation): -2.36 ± 0.01 kHz/N, -2.36 ± 0.01 kHz/N, and -1.75 ± 0.03 kHz/N, respectively. These slopes indicated that the excitation of the strain gauge had no effect on the ARF of the antenna, but the removal of the strain gauge produced a 26% decrease in the ARF per load slope.

The finite element simulation of this experiment predicted an average tensile principal strain of 1340 $\mu\varepsilon\pm$ 58 $\mu\varepsilon$ on the plate under a global 500 N compressive load. This prediction represented a 1% difference from the average experimental result. The relative deflection of the plate under the 500 N load was predicted to be 0.58 mm. The electromagnetic computational simulations matched the experimental ARF very well (Fig. 6b); there were 0.03% and 0.05% differences in the ARF between the experiment and model predictions of the undeformed and deformed configurations, respectively. The ARF shift due to the applied 500 N load in the experimental data and model predictions were 0.9 MHz and 1.0 MHz, respectively, which corresponds to an 11% difference. The model used in the electromagnetic simulations did not include the cable that connects the antenna to the network analyzer, which explains the discrepancy in the actual $|S_{11}|$ levels (with regard to signal strength, dB). Namely, due to the insertion of the feeding cable, the experimental setup included more losses (*i.e.*, away from the resonances experimental curves were about 1 dB lower than the simulated curves).

VI. DISCUSSION

The three experimental tests and accompanying computational modelling analyses in the current study have demonstrated the efficacy of the DEC method to sense near-field displacements of a metal plate and plate deflection due to a mechanical load. The parametric tests of plate placement on the antenna and cable spacing guided the design of an antenna to optimize its sensitivity (shifts in resonant frequency due to displacements of a metal plate). The antenna design was tested and validated through the plate displacement and plate compression tests, along with the corresponding computational models.

The parametric test on plate placement along the antenna length demonstrated how the location(s) of greatest sensitivity depended on the harmonic resonant frequency measured. These results formed the foundation for the concept of aligning the three sensitive locations of the third harmonic frequency for the coiled antenna design. By aligning these three locations, the effects of shifting ARF due to the plate displacements were combined for a single configuration, creating a drastic increase in the sensitivity of the antenna.

The parametric test on cable spacing demonstrated a general increase in sensitivity with increased spacing, as determined by the c parameter of the inverse square model fits (Fig. 3a) and the overall ARF shift between 0 and 30 mm displacements (Fig. 3c). When comparing normalized ARF shifts (Fig. 3c) and the signal/noise ratio (Fig. 3d), there didn't appear to be a substantial effect of changing harmonic frequencies. However, using the third harmonic frequency allowed for the coiled antenna concept, which greatly improved the antenna's sensitivity. Although the results indicated that it would be desirable to maximize the antenna spacing (within the tested range of 10 mm to 40 mm), the design

of the coiled antenna was restricted by size requirements for the intended use of sensing plate deformations in fractured bones.

On the coiled antenna, the outer shield of the coaxial line essentially behaves as a coiled dipole arm. In the presented setup, the circumference of the top turn of the two coils (about 348.5 mm), is about one half of the guided wavelength on the outer shield at 430 MHz. This puts the minima of the current along the arm (which are one quarter of the guided wavelength away from the feeding point where the two coils are connected to each other) closely at one half of the turns, or directly opposite to the feeding point. Noting that this is also the position where the metal plate is situated in the antenna vicinity, its introduction efficiently loads the antenna arm capacitively. The loading increases the antenna effective length and, in turn, lowers its resonant frequency. As the metallic plate nears the antenna, the capacitive loading becomes more pronounced, thus ultimately lowering further the antenna resonant frequency.

Similar to the parametric tests on spacing, the plate displacement test established that the final antenna design can sense (as a shift in ARF) displacements of a metal plate in the near field. The orthopaedic plate compression test established that the antenna can effectively sense the deflection of a plate due to an applied load in a configuration closely resembling a long bone with a transverse fracture. The mechanical finite element simulation mirrored the experimental test; as expected, the plate experienced a lateral bending deflection when compressively loaded (which induced a bending moment due to the offset of the compression). Although the antenna's ARF exhibited a nonlinear (inverse square) relationship with the plate displacement over a large displacement range (Fig. 5c) in the plate displacement test, the plate compression test demonstrated that over the approximately 0.5 mm deflection range, the relationship between ARF and applied load was highly linear (Fig. 6c).

The electromagnetic modeling predictions closely matched the experimental data in both the plate displacement and plate compression tests, further supporting the theoretical foundation of the DEC method. The close agreement of the electromagnetic modeling predictions strongly support the validity of the developed model. The small difference between experimental and modeling results is likely due to simplifications of the physical environment made in the electromagnetic model (*e.g.* the feeding cable, the table top, and the clamps holding the antenna in the experiment were not included in the model). The electromagnetic models developed in the current study will be utilized to further optimize the antenna design and measurement setup to improve the sensitivity and reliability of the DEC measurement system. Only the coaxial dipole antenna type was tested in the current study. Further improvements could be made by investigating other antenna types and conducting further parametric studies.

A limitation of the DEC system is that it requires a highly controlled environment. Changes in location of the antenna relative to the target object can affect its performance. Environmental sources of error can also be introduced, such as the movement of people or other objects in the vicinity of the antenna. Applying this technique in a reliable measurement system will require methods in place to ensure a repeatable antenna placement and stable environmental conditions.

VII. CONCLUSIONS

The antenna is intended to be used in a diagnostic measurement system to sense deflections of a fractured bone fixed with orthopaedic hardware (*e.g.* a plate with corresponding screws or an intramedullary nail with corresponding pins), and to track changes in the measurement over time throughout the healing process. The current study established the foundation of this measurement system to sense plate deflections due to an applied load causing the plate to bend. An additional study by our group using the same antenna on sheep long bones has demonstrated the measurement system's ability to detect changes in the mechanical load sharing between the plate and fracture site that are representative of a fracture healing over time [32]. Therefore, this measurement system has potential to provide valuable diagnostic information regarding the progression of fracture healing. This type of sensor may have potential utility in other applications where it is desirable to sense the deflection or displacement of a mechanical component.

REFERENCES

[1] A. Praemer, S. Furner, and D. Rice, "Musculoskeletal conditions in the United States. Park Ridge, Il," Amer. Acad. Orthopaedic Surgeons, Rosemont, IL, USA, Tech. Rep., 1999.

[2] P. V. Giannoudis, Z. Dahabreh, and R. I. Dimitriou, "The cost of treatment of fracture non-unions using recombinant bone morphogenic protein 7," Amer. Acad. Orthopaedic Surgeons, Rosemont, IL, USA, Tech. Rep., 2006.

[3] R. Schmidhammer *et al.*, "Assessment of bone union/nonunion in an experimental model using microcomputed technology," *J. Trauma*, vol. 61, no. 1, pp. 199–205, Jul. 2006.

[4] K. Dickson, S. Katzman, E. Delgado, and D. Contreras, "Delayed unions and nonunions of open tibial fractures. Correlation with arteriography results," *Clin. Orthopaedics Rel. Res.*, vol. 302, pp. 189–193, May 1994.

[5] T. Miclau *et al.*, "Effects of delayed stabilization on fracture healing," *J. Orthopaedics Res.*, vol. 25, no. 12, pp. 1552–1558, Dec. 2007.

[6] Z. Thompson, T. Miclau, D. Hu, and J. A. Helms, "A model for intramembranous ossification during fracture healing," *J. Orthopaedics Res.*, vol. 20, no. 5, pp. 1091–1098, Sep. 2002.

[7] K. Stoffel, K. Klaue, and S. M. Perren, "Functional load of plates in fracture fixation *in vivo* and its correlate in bone healing," *Injury*, vol. 31, no. 2, pp. 37–50, May 2000.

[8] B. S. Klosterhoff *et al.*, "Wireless implantable sensor for noninvasive, longitudinal quantification of axial strain across rodent long bone defects," *J. Biomechan. Eng.*, vol. 139, no. 11, p. 111004, Nov. 2017.

[9] R. Melik, N. K. Perkgoz, E. Unal, C. Puttlitz, and H. V. Demir, "Bio-implantable passive on-chip RF-MEMS strain sensing resonators for orthopaedic applications," *J. Micromech. Microeng.*, vol. 18, no. 11, p. 115017, Nov. 2008.

[10] R. Melik, E. Unal, N. K. Perkgoz, C. Puttlitz, and H. V. Demir, "Circular high-Q resonating isotropic strain sensors with large shift of resonance frequency under stress," *Sensors*, vol. 9, no. 12, pp. 9444–9451, Dec. 2009.

[11] R. Melik, E. Unal, N. K. Perkgoz, C. Puttlitz, and H. V. Demir, "Flexible metamaterials for wireless strain sensing," *Appl. Phys. Lett.*, vol. 95, no. 18, p. 181105, Nov. 2009.

[12] R. Melik, E. Unal, N. K. Perkgoz, C. Puttlitz, and H. V. Demir, "Metamaterial-based wireless strain sensors," *Appl. Phys. Lett.*, vol. 95, no. 1, p. 011106, Jul. 2009.

[13] R. Melik, E. Unal, N. K. Perkgoz, C. Puttlitz, and H. V. Demir, "Metamaterial based telemetric strain sensing in different materials," *Opt. Express*, vol. 18, no. 5, pp. 5000–5007, Mar. 2010.
[14] R. Melik, E. Unal, N. K. Perkgoz, C. Puttlitz, and H. V. Demir, "Metamaterial-based wireless RF-MEMS strain sensors," in *Proc. IEEE Sensors*, Nov. 2010, pp. 2173–2176.
[15] R. Melik, E. Unal, N. K. Perkgoz, C. Puttlitz, and H. V. Demir, "RF-MEMS load sensors with enhanced Q-factor and sensitivity in a suspended architecture," *Microelectron. Eng.*, vol. 88, no. 3, pp. 247–253, Mar. 2011.
[16] R. Melik *et al.*, "Nested metamaterials for wireless strain sensing," *IEEE J. Sel. Topics Quantum Electron.*, vol. 16, no. 2, pp. 450–458, Mar./Apr. 2010.
[17] B. Ozbey *et al.*, "Wireless displacement sensing enabled by metamaterial probes for remote structural health monitoring," *Sensors*, vol. 14, no. 1, pp. 1691–1704, 2014.
[18] K. C. McGilvray *et al.*, "Implantable microelectromechanical sensors for diagnostic monitoring and post-surgical prediction of bone fracture healing," *J. Orthopaedics Res.*, vol. 33, no. 10, pp. 1439–1446, Oct. 2015.
[19] E. H. Ledet, B. Liddle, K. Kradinova, and S. Harper, "Smart implants in orthopedic surgery, improving patient outcomes: A review," *Innov. Entrepreneurship Health*, vol. 5, pp. 41–51, Jan. 2018.
[20] X. Qing and Z. N. Chen, "Proximity effects of metallic environments on high frequency RFID reader antenna: Study and applications," *IEEE Trans. Antennas Propag.*, vol. 55, no. 11, pp. 3105–3111, Nov. 2007.
[21] P. R. Foster and R. A. Burberry, "Antenna problems in RFID systems," presented at the Inst. Elect. Eng. Colloq. RFID Technol., 1999.
[22] D. M. Dobkin and S. M. Weigand, "Environmental effects on RFID tag antennas," in *IEEE MTT-S Int. Microw. Symp. Dig.*, vols. 1–4, Jun. 2005, pp. 135–138.
[23] G. S. Smith, "Directive properties of antennas for transmission into a material half-space," *IEEE Trans. Antennas Propag.*, vol. AP-32, no. 3, pp. 232–246, Mar. 1984.
[24] J. D. Griffin, G. D. Durgin, A. Haldi, and B. Kippelen, "RF tag antenna performance on various materials using radio link budgets," *IEEE Antennas Wireless Propag. Lett.*, vol. 5, no. 1, pp. 247–250, Dec. 2006.
[25] W. Amer, G. Y. Tian, and C. Tsimenidis, "Sensing passive object existence within an antenna near field based on return loss," in *Proc. Loughborough Antennas Propag. Conf. (LAPC)*, Nov. 2014, pp. 400–404.
[26] S. Fericean and R. Droxler, "New noncontacting inductive analog proximity and inductive linear displacement sensors for industrial automation," *IEEE Sensors J.*, vol. 7, no. 11, pp. 1538–1545, Nov. 2007.
[27] P. Kejík, C. Kluser, R. Bischofberger, and R. S. Popovic, "A low-cost inductive proximity sensor for industrial applications," *Sens. Actuators A, Phys.*, vol. 110, nos. 1–3, pp. 93–97, 2004.
[28] B. M. Notaros, *Electromagnetics*. Upper Saddle River, NJ, USA: Prentice-Hall, 2011, p. XVII-815.
[29] M. M. Ilic and B. M. Notaros, "Higher order hierarchical curved hexahedral vector finite elements for electromagnetic modeling," *IEEE Trans. Microw. Theory Techn.*, vol. 51, no. 3, pp. 1026–1033, Mar. 2003.
[30] S. V. Savić, B. M. Notaroš, and M. M. Ilić, "Accuracy analysis of the nonrigorous second-order absorbing boundary condition applied to large curved finite elements," in *Proc. Int. Conf. Electromagn. Adv. Appl. (ICEAA)*, Sep. 2015, pp. 58–61.
[31] R. Pethig, "Dielectric properties of body tissues," *Clin. Phys. Physiol. Meas.*, vol. 8, no. 4A, pp. 5–12, 1987.
[32] K. M. Labus *et al.*, "Direct electromagnetic coupling for non-invasive diagnostic monitoring and predition of bone fracture healing," *J. Orthopaedic Res.*, 2018.

KEVIN M. LABUS was born in Indianapolis, IN, USA. He received the B.S. degree in mechanical engineering from the University of Notre Dame, Notre Dame, IN, USA, in 2011, and the Ph.D. degree in bioengineering from Colorado State University, Fort Collins, CO, USA, in 2016.

From 2016 to 2018, he was a Post-Doctoral Research Fellow, and since 2018, he has been a Research Scientist with the Orthopaedic Bioengineering Research Laboratory, Mechanical Engineering Department, Colorado State University. His research interests include experimental and computational biomechanics with applications in fracture healing, spine, other orthopaedic systems, and neural tissue.

BRANISLAV M. NOTAROŠ (M'00–SM'03–F'16) received the Dipl.Ing. (B.S.), M.S., and Ph.D. degrees in electrical engineering from the University of Belgrade, Belgrade, Yugoslavia, in 1988, 1992, and 1995, respectively.

From 1996 to 1999, he was an Assistant Professor with the School of Electrical Engineering, University of Belgrade. From 1998 to 1999, he was a Visiting Scholar with the University of Colorado at Boulder. He was an Assistant Professor, from 1999 to 2004, and an Associate Professor, from 2004 to 2006, with the Department of Electrical and Computer Engineering, University of Massachusetts Dartmouth. From 2006 to 2012, he was an Associate Professor with the Department of Electrical and Computer Engineering, Colorado State University (CSU), where he is currently a Professor and a University Distinguished Teaching Scholar, and the Director of the Electromagnetics Laboratory. He has authored textbooks *Electromagnetics* (Prentice Hall, 2010), *MATLAB-Based Electromagnetics* (Prentice Hall, 2013), and *Conceptual Electromagnetics*(CRC Press, 2017). His research interests and activities are in computational electromagnetics, higher order numerical methods, antennas, scattering, microwaves, metamaterials, characterization of snow and rain, surface and radar precipitation measurements, RF design for MRI at ultra-high magnetic fields, and electromagnetics education.

Dr. Notaroš is a fellow of the Applied Computational Electromagnetics Society (ACES). He was a recipient of the 2005 IEEE MTT-S Microwave Prize (Best-Paper Award for the IEEE Transactions on Microwave Theory and Techniques), the 1999 IEE Marconi Premium (Best-Paper Award for IEE Proceedings on Microwaves, Antennas and Propagation), the 1999 the International Union of Radio Science (URSI) Young Scientist Award, the 2005 UMass Dartmouth Scholar of the Year Award, the 2004 UMass Dartmouth College of Engineering Dean's Recognition Award, the 2010 CSU College of Engineering George T. Abell Outstanding Teaching and Service Faculty Award, the 2012 CSU System Board of Governors Excellence in Undergraduate Teaching Award, the 2012 IEEE Region 5 Outstanding Engineering Educator Award, the 2014 CSU Provost's N. Preston Davis Award for Instructional Innovation, the 2014 Carnegie Foundation for the Advancement of Teaching Colorado Professor of the Year Award, the 2015 American Society for Engineering Education ECE Distinguished Educator Award, and the 2015 IEEE Undergraduate Teaching Award. He serves as the Vice-Chair for the U.S. National Committee Commission B of URSI, for which he previously served as a Technical Activities Chair (2015–2018). He served as the General Chair of the 2018 International Applied Computational Electromagnetics Society Symposium–ACES2018, Denver, CO, USA, in 2018, and of the 11th International Workshop on Finite Elements for Microwave Engineering–FEM2012, Estes Park, CO, USA, in 2012. He serves as the General Chair for the 14th International Workshop on Finite Elements for Microwave Engineering–FEM2018, Cartagena de Indias, Colombia, in 2018. He is an Associate Editor for the IEEE Transactions on Antennas and Propagation, and served as a Guest Editor for the Special Issue on Finite Elements for Microwave Engineering, Electromagnetics, vol. 34, issue 3–4, in 2014. He serves on the Board of Directors for ACES and as an ACES Secretary.

MILAN M. ILIĆ (S'00–M'04–SM'18) received the Dipl.Ing. and M.S. degrees in electrical engineering from the University of Belgrade, Serbia, in 1995 and 2000, respectively, and the Ph.D. degree from the University of Massachusetts Dartmouth, USA, in 2003.

He is currently a Professor with the School of Electrical Engineering, University of Belgrade, and an Affiliated Faculty with the ECE Department, Colorado State University, USA. His research interests include computational electromagnetics, antennas, magnetic resonance imaging, and microwave electronics.

Dr. Ilić was a recipient of the 2005 IEEE MTT-S Microwave Prize.

CONOR J. SUTHERLAND was born in Dunedin, New Zealand, in 1995. He received the B.Eng. degree (Hons.) in mechanical engineering from the University of Canterbury, Christchurch, New Zealand, in 2016. He currently pursuing the degree in mechanical engineering with Colorado State University, Fort Collins, USA.

He was a Researcher with the University of Canterbury in 2016. He has previously been involved in research involving neonatal ventilation and craniofacial hardware. He now focuses on monitoring fracture healing in long bones via the use of both experimental and CAE methods.

AMY HOLCOMB received the dual B.S. degrees in mechanical engineering and biomedical engineering from Colorado State University, Fort Collins, CO, USA, in 2018.

From 2016 to 2018, she was an Undergraduate Research Assistant with the Orthopaedic Bioengineering Research Laboratory, Mechanical Engineering Department, Colorado State University. She is currently involved with virtual surgical planning for oral and dental surgery for Guided Surgical Solutions, Denver, CO, USA. Other interests of hers include computational biomechanics, virtual surgical planning, and backpacking.

CHRISTIAN M. PUTTLITZ received the B.S. degree in material science and engineering mechanics from Michigan State University in 1992, the M.S. degree in bioengineering from Clemson University in 1993, and the Ph.D. degree in biomedical engineering from The University of Iowa in 1999.

He went on to become a Post-Doctoral Fellow with the Orthopaedic Bioengineering Research Laboratory, University of California at San Francisco (UCSF), San Francisco. He joined the Department of Orthopaedic Surgery Faculty, UCSF, in 2001, as an Assistant Professor, directed the Orthopaedic Biomechanics Laboratory, San Francisco General Hospital, and was a participating faculty in the UCSF/UC Berkeley Graduate Program in bioengineering. In 2005, he accepted a faculty position at the Department of Mechanical Engineering, Colorado State University (CSU), and is currently appointed as a Full Professor. He also holds secondary appointments with the School of Biomedical Engineering and the Department of Clinical Sciences, CSU.